JOURNAL OF AEROSPACE COMPUTING, INFORMATION, AND COMMUNICATION
Vol. 6, April 2009

Terrain Elevation Data Integrity Monitor and Referenced Navigation

Ananth K. Vadlamani* and Maarten Uijt de Haag†
Ohio University, Athens, Ohio 45701

DOI: 10.2514/1.39689

Synthetic vision systems provide a synthesized view of the outside world to pilots on displays in the flight deck. Terrain databases onboard aircraft are used as the source of terrain elevation information on synthetic vision system displays. Because the primary function of these displays is to improve flight safety, it is imperative that the terrain data used to generate the imagery conform to a high level of integrity. Otherwise, instead of preventing accidents, the terrain database would be cause of more. Hence, it is necessary to include an integrity monitor function that ensures the terrain data are consistent with the real world. In this paper, we revisit previously proposed concepts and present the development of a 3D spatial data integrity monitor. The framework is also extended to a terrain referenced navigation scheme such that both operations can be performed simultaneously. Presented furthermore is a Kalman filter design and its associated tradeoffs for improving the performance of the integrity monitor and navigation functions. The performance of the integrity monitor and position estimator for navigation is evaluated using flight test data collected in the vicinity of Braxton County airport in West Virginia.

I. Introduction

ONE of the challenges faced by pilots is maintaining proper flight operations during reduced visibility conditions. Reduced visibility may occur as a result of adverse weather conditions such as clouds, rain, fog or snow and darkness. These scenarios are termed instrument meteorological conditions (IMC) when a pilot must rely on instruments and other navigation aids rather than an out-of-the-window view to continue with flight operations. During high dynamics flight, the human body's natural capability to sense and align with the Earth's gravity is also diminished. Although most aircraft are equipped with instruments to aid the pilot in IMC, they do not provide a sense of situational awareness (SA), which is the reason synthetic vision systems (SVS) are being developed. The primary goals of SVS are to help maintain spatial orientation and improve situational awareness. Hence, SVS may reduce the number of controlled flight into terrain (CFIT) accidents [1], a scenario wherein a pilot crashes into terrain, water, or obstacles even while commanding complete control over the aircraft.

A. Motivation

The source for the terrain information depicted on the SVS display is a digital elevation model (DEM) or terrain database. SVS displays provide a clear, daylight view of the outside world at all times, even in poor visibility

Received 10 July 2008; accepted for publication 09 September 2008.

* Graduate Research Associate, Department of Electrical Engineering and Computer Science, 231 Stocker Center, Ohio University, av138901@ohio.edu

† Associate Professor, Department of Electrical Engineering and Computer Science, 321B Stocker Center, Ohio University, uijtdeha@ohio.edu, AIAA Senior Member.

conditions. Because of the compelling nature of the displays, it is possible for the pilots to use the displays for functions other than what they are designed for. This is referred to as the "unintended use" of SVS displays. Under such circumstances, the terrain database or DEM must be guaranteed to a high level of integrity. For a system that is meant to improve aviation safety, SVS must meet or exceed the required reliability ratings based on the derived fault tree analyses (FTAs) and other safety assessment tools. The SVS includes the terrain database server, and to ensure that the terrain elevation data meets the required reliability, an integrity monitor function may be added to the terrain database server that would guarantee the specified probabilities of fault-free detection (false alarm) and of missed detection. An integrity monitor, designed within the statistical framework of these probabilities must alert the flight crew, should a systematic error exist in the terrain database.

Terrain database integrity monitors (TDIM) that use a downward-looking sensor such as a radar altimeter and global positioning system (GPS) inputs have been proposed in [2,3]. The integrity monitor is an algorithm that performs a consistency check between the terrain database and sensor measurements of the real world, from a statistical perspective. In this paper, we examine the integrity of terrain data from the aspect of a bias error. In the presence of a bias error, the SVS may display hazardously misleading information (HMI) in the form of incorrect terrain clearances or incorrect aircraft position relative to a terrain feature (mountains, for example). In such cases, in addition to raising an integrity alert, we can go a step further and correct the display imagery by estimating the aircraft position with respect to the biased database. This leads us to the terrain database-referenced navigation (TDRN) scheme presented here. The dual functions of TDIM and TDRN can be performed simultaneously because both systems are based on performing a comparison between onboard stored data and data obtained, independently, from airborne sensors such as a radar altimeter, inertial measurement unit (IMU), and/or a GPS receiver.

B. Digital Elevation Models

A digital elevation model or terrain database is a digital look-up table containing terrain heights corresponding to their horizontal position coordinates (e.g. latitude and longitude), expressed in a pre-defined datum. Examples of DEMs are the digital terrain elevation database (DTED) levels 0, 1 and 2, Jeppesen terrain databases and shuttle radar topography mission (SRTM) terrain data. DEM specifications consist of various parameters such as resolution (or data density), the horizontal and vertical reference datums, and linear and circular error probabilities [4]. The linear error specifies the accuracy in the vertical direction whereas the circular error specifies the accuracy in the horizontal direction. An illustration of linear and circular errors is shown in Fig. 1 [5].

Ideally, a DEM should represent the terrain elevation at corresponding horizontal coordinates. However, the database elevations deviate from the true elevations owing to systematic faults and randomly distributed errors that get introduced in the DEM primarily owing to the way in which they are generated from different sensor technologies such as photogrammetry, remote sensing and so on, coordinate transformation mismatches, discrepancies in vertical and horizontal datums used to express the coordinates and also owing to manual post-processing errors.

The terrain database errors are in the form of:

- biases in the vertical and horizontal domains;
- ramps in the vertical and horizontal domains;
- randomly distributed errors in the vertical domain and circularly distributed random errors in the horizontal domain.

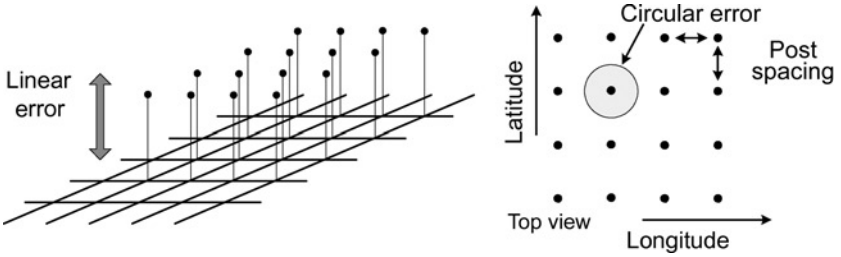

Fig. 1 DEM linear and circular errors.

In this paper, we consider bias errors in both the vertical and horizontal domains. Biases in a DEM larger than a nominal level are considered DEM failures. Because of the inherent presence of sensor measurement noise and random errors in the DEM, it is not possible to detect vertical biases and horizontal translations in an absolute sense, but only in a statistical manner.

C. Prior Work and Current Effort

Various sensors have been considered to support the integrity monitor function. Earlier work [2,3,5,6] has used a downward-looking radar altimeter because most aircraft are already equipped with one. The applicability of light detection and ranging (LIDAR) was investigated in [7] and forward-looking, X-band weather radar, configured in terrain mapping mode is used in [8].

In terrain-referenced navigation (TRN), external sensors are integrated with terrain databases to obtain position and/or velocity estimates. Among the various terrain navigation methods, terrain contour matching (TERCOM) [9,10] is a method of terrain navigation in which the vehicle's position is derived by correlating a sensed terrain profile (synthesized from radar altimeter measurements) to a map terrain profile. The resulting position is input to a Kalman filter that updates the vehicle's inertial navigation system (INS). In Sandia inertial terrain-aided navigation (SITAN) [10–12] the INS is aided using terrain slope information as an input to a Kalman filter instead of terrain profile correlation. Use of a log-likelihood function of the discrepancy between changes along the sensed and map terrain profiles is investigated in [13].

This paper is an extension of work previously done by Ohio University and presented in [14–17]. Although the basic concepts introduced in those works are summarized here, the reader is referred to those works for an extensive treatment as well as various other flight test results. This paper is organized as follows: The spatial integrity monitor concept is presented in Sec. II. Section III reviews some basic statistics that help in formulating the integrity monitor in Sec. IV. Detailed results are provided in Sec. V based on flight tests conducted in the vicinity of Braxton county Airport (K48I) in West Virginia aboard Ohio University's Douglas DC-3 aircraft. Spatial position estimation and bias definitions for TDRN are presented in Sec. VI followed by their results in Sec. VII.

II. Spatial Integrity Monitor Concept

The terrain database integrity monitor performance is specified by the probability of fault–free detection (P_{FFD}), probability of missed detection (P_{MD}) and time-to-alarm. The TDIM uses the aircraft radar altimeter as its primary sensor for measuring ground clearance. The radar altimeter measurements, along with GPS-derived aircraft heights are used to synthesize terrain elevations which are compared with the database elevations. The difference between the synthesized and database height is referred to as the *sample disparity*. The integrity monitor is formulated to primarily detect vertical biases in the disparities. Inherent to the statistical nature of the algorithm, the TDIM may flag an integrity alarm even when a bias does not exist. This condition is referred to as "fault-free detection" or "false alarm". Similarly, small values of a bias may go undetected leading to a condition known as a "missed detection". If the magnitude of the bias is such that it falls below the noise level of the sensor measurements, there exists a high probability for missed detections. Given predefined probabilities of fault-free and missed detections, we can now define a 3D grid of possible aircraft positions that would result in our proposed algorithm to miss a terrain database failure, even if such a failure did exist. This grid is termed the "Spatial Envelope" of missed detection. This concept is illustrated in Fig. 2. The 2D horizontal equivalent is called the region of missed detection (RMD).

Only the lower half of the spatial envelope is shown in Fig. 2 because the terrain is below the aircraft and, thus, only the lower half is significant for generating a CFIT alert. A similar upper half exists, having decreasing RMD with increasing magnitude of a positive vertical bias. The spatial envelope of missed detection signifies the volume within which the probability of a missed detection is larger than or equal to the required probability of missed detection, or, in physical terms, an aircraft present anywhere within that volume fails to generate a vertical domain terrain database bias/integrity alert. Hence, to maintain safe operation, an integrity alert should definitely be generated if any part of spatial envelope intersects the actual terrain. The extent of the spatial envelope depends on the roughness and nonperiodicity of the terrain features. While relying on the terrain for situational awareness, the spatial envelope of missed detection is also an indication of the aircraft's position uncertainty.

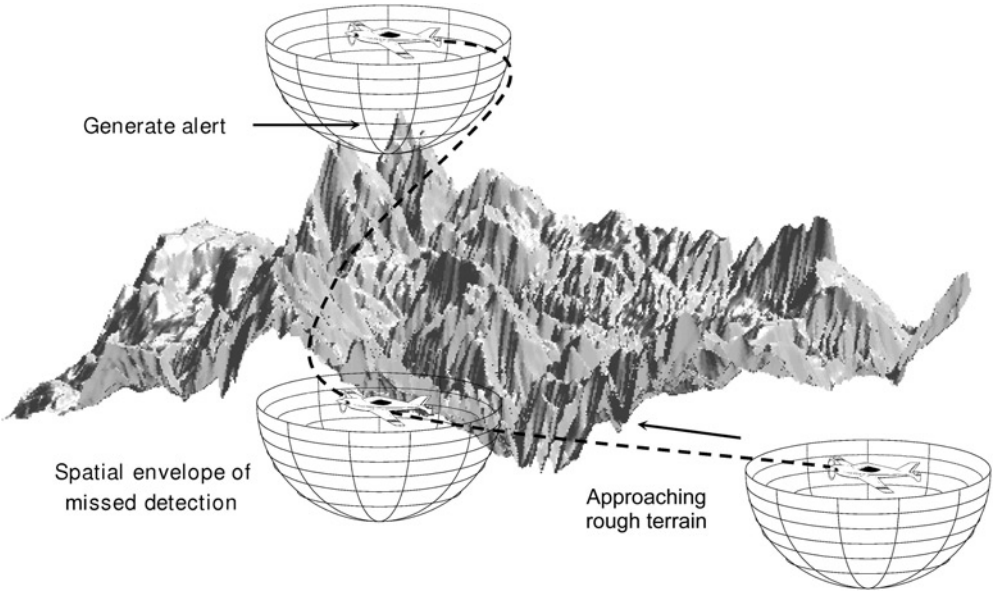

Fig. 2 Spatial integrity monitor and the concept of a "spatial envelope" of missed detection.

III. Statistical Background

The difference between the synthesized and the database elevations are known as sample disparities and will, under ideal conditions, look like random noise. Consider a random set of sample disparities of size N, $x_1, x_2, \ldots, x_n$, taken from a normal population N(μ, σ^2)having mean μ and variance σ^2. Because the samples are normally distributed, their squares, $x_1^2, x_2^2, \ldots, x_n^2$, are distributed according to a χ^2 distribution [18]. Then

$$\chi^2 = \frac{1}{\sigma^2}\sum_{i}^{N}(x_i - \mu)^2 \tag{1}$$

is a random variable (RV) having a χ^2 distribution with N degrees of freedom. The quantity χ^2 is widely used in detection theory when making a statistical decision between two or more hypotheses.

A. Formulation of Hypotheses

Our approach to integrity monitoring is founded on basic detection theory and uses the following hypothesis testing steps [18]:

1. Formulate a null hypothesis ($\mathbf{H_0}$) and an appropriate Alternate Hypothesis ($\mathbf{H_1}$) that is accepted when the null hypothesis is rejected.
2. Specify the probability of a type I error for $\mathbf{H_0}$; if necessary, also specify the probability of a type II error for $\mathbf{H_1}$. (These errors are defined below.)
3. Based on the sampling distribution of an appropriate statistic, construct a criterion for testing the null hypothesis against the given alternative hypothesis.
4. Calculate from the data, the value of the test statistic on which the decision is to be based.
5. Compare the test statistic with the criterion and decide whether to reject the null hypothesis, accept it or to reserve judgment.

Rejecting the null hypothesis $\mathbf{H_0}$ while it is true is referred to as either a type I error or a fault-free detection or false alarm. Acceptance of hypothesis $\mathbf{H_0}$ while it is false is referred to as type II error or a missed detection. These error types are shown in Table 1.

Under the fault-free condition (no bias), the over-bounding probability density function (PDF) of the errors on both the sensors and the terrain database can be represented by a normal PDF, leading to the following null hypothesis

Table 1 Decision making in hypothesis testing

	Accept H_0	Reject H_0
H_0 is true	Correct decision	Type I error (Fault-free detection)
H_0 is false	Type II error (Missed detection)	Correct decision

or fault-free hypothesis:

$$\mathbf{H_0} : x \sim \mathbf{N}(0, \sigma^2) \tag{2}$$

where $\mathbf{N}(0, \sigma^2)$ is a normal distribution with mean zero and variance σ^2. The variance σ^2 is computed by summing the variances of the individual sensor errors and the nominal terrain database errors. These errors include errors owing to ground cover and the specified error characteristics of the DEM [2].

When a failure mode exists in the form of a bias (on the terrain database elevations), the bias shows up in the PDF as a nonzero mean value of the normal samples, giving rise to the following alternate or faulted hypothesis:

$$\mathbf{H_1} : x \sim \mathbf{N}(\mu, \sigma^2) \tag{3}$$

where μ is the failure bias. Furthermore, the minimum detectable bias, μ_B, is defined as the smallest bias that can be detected with a probability of $1 - P_{\text{MD}}$.

Under $\mathbf{H_0}$, the χ^2 statistic (henceforth referred to as the T-value or T) of Eq. (1) is χ^2 distributed with N degrees of freedom, whereas, under $\mathbf{H_1}$, T follows a noncentral χ^2 distribution with N degrees of freedom and noncentrality parameter λ. Figure 3 shows a representation of the distributions of the test statistic, T, under the $\mathbf{H_0}$ and $\mathbf{H_1}$ hypotheses [6].

Given values for the probability of fault-free detection, P_{FFD}, and number of samples, N, the decision threshold value, T_{th}, for T can be computed. The decision between $\mathbf{H_0}$ and $\mathbf{H_1}$ can now be defined as follows:

$$\begin{aligned} \mathbf{H_0} &: T \leqslant T_{th} \\ \mathbf{H_1} &: T > T_{th} \end{aligned} \tag{4}$$

Given the threshold value, T_{th}, and the probability of missed detection, P_{MD}, a corresponding noncentrality parameter, λ_B, can be computed for the faulted PDF ($\mathbf{H_1}$) [16]. Now, the minimum detectable bias μ_B can be computed

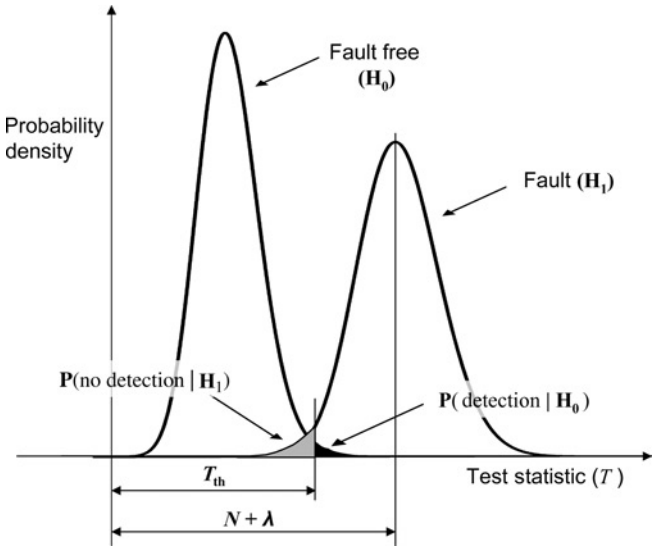

Fig. 3 Distribution of T for $\mathbf{H_0}$ and $\mathbf{H_1}$.

from λ_B as follows [6,19]:

$$\mu_B = \sigma\sqrt{\frac{\lambda_B}{N}} \tag{5}$$

B. Kalman Filter Formulation

A Kalman filter is used on the sample disparities to reduce the nominal noise owing to the sensors and terrain database and to estimate a potential bias error present on the sensors and terrain database combined. If the nominal errors are Gaussian, the Kalman filter is an optimal estimator for the bias error in the minimum mean squared error (MMSE) sense. The system model for the Kalman filter is given by a bias component and a noise component or $z = \mu + \eta$ where, $\eta \in \mathbf{N}(0, \sigma^2)$. Here, the filter estimates the bias component μ while reducing the noise; hence, the state vector is simply a scalar. We limit ourselves to a basic Kalman filter formulation [20] to illustrate the performance of the integrity monitor and navigation scheme. The filter is initialized using the following parameters:
$\hat{x}_0^-$, the initial state prediction is zero as per the assumed system model,
P_0^-, the initial prediction error variance can be a value, roughly between $(15)^2$ and $(20)^2$,
ϕ_k, the state transition matrix equal to unity,
z_k, is the measurement input to the Kalman filter at time t_k; sample disparity identical with $x(t_k)$,
H_k, is the state-to-measurement domain transformation matrix; unity,
R_k, is the measurement error variance; $(18.9)^2$, constant (refer Table 2),
Q_k, is the system noise variance, also called the tuning parameter of the filter, constant in our implementation.

Based on the choice for the tuning parameter Q, the variance of the estimates, P, attains a constant steady-state value over time. The steady-state value of P is assumed to be the population variance of the filtered estimates of the sample disparities, if the filter were evaluated for aircraft positions covering the entire terrain database. After convergence, σ in Eq. (5) can be substituted by $\sqrt{P}$ and the corresponding minimum detectable bias, μ_B for the Kalman filtered case can be computed. Or vice-versa, given a required value of μ_B, the desired estimator variance P can be computed and the tuning parameter Q can be determined by Kalman covariance analysis simulation. Figure 4 shows a plot of both P and Q as a function of the minimum detectable bias μ_B.

Table 2 Overbounded absolute disparity distributions for sensors and data [2]

Vertical error source	Absolute disparity distribution
Radar altimeter	$\mathbf{N}(0, (1.8)^2)$
Kinematic GPS height	$\mathbf{N}(0, (0.22)^2)$
DTED vertical error	$\mathbf{N}(0, (18.2)^2)$
Ground cover	$\mathbf{N}(0, (4.6)^2)$
Convolved distribution (σ)	$\mathbf{N}(0, (18.9)^2)$

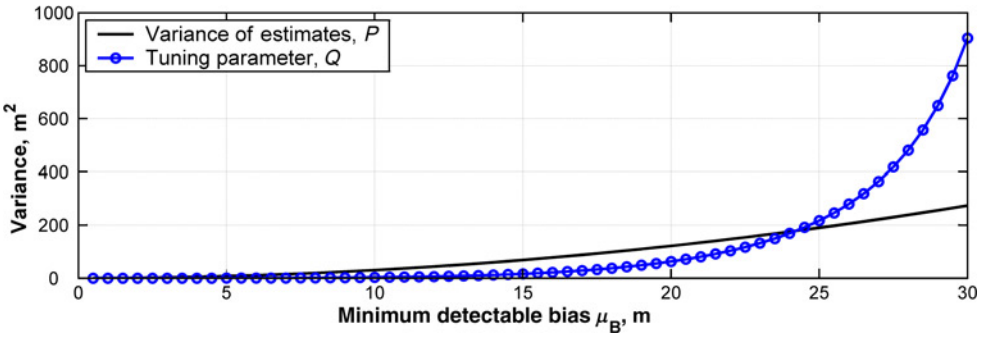

Fig. 4 Kalman variances P and Q as a function of μ_B.

However, filtering of the sample disparities invalidates the basic assumption used in Eq. (1) that the underlying random variables, x_i, are independent and identically distributed (IID). The filtered estimates are correlated and therefore Eq. (1) no longer applies in a strict sense. The amount of correlation of the estimator outputs, in time, depends on the filter's tuning parameter, Q. For relatively large values of Q (and thus μ_B), Eq. (1) still applies without violating the independency assumption. For the Kalman filter implementation, we chose $\mu_B = 25$ m ($\sim$10 m lower than the unfiltered disparity case and explained in the next section). Monte-Carlo analyses have shown that for $\mu_B = 25$ m and its corresponding Q-value, the filtered disparities have a de-correlation time of approximately 5–6 s. Hence, suppose every fifth sample were picked from the Kalman filter output and input to the Integrity Monitor, the monitor inputs could still be considered independent. However, this would reduce the degrees of freedom in Eq. (1) by a factor of 5. Thus, to maintain the same number of degrees of freedom, the number of original samples must be increased five-fold. Such an increase in samples would result in a time-to-alert which is five times longer than the original time-to-alert. In our implementation, the radar altimeter operates at a measurement rate of 25 Hz. So, we picked a sample every five measurements to enable a one-to-one comparison of the unfiltered and filtered cases.

IV. Terrain Database Integrity Monitor: In 1, 2, and 3 Dimensions

In this section, we describe the design of the integrity monitor in the vertical domain and then expand it to the horizontal (2D) and the spatial (3D) domain.

A. Vertical Domain Integrity Monitor

The vertical domain integrity monitor concept was originally proposed in [2], and compares the terrain database elevation profile with an independent terrain profile synthesized from a downward-looking external sensor, in real-time. The method uses a Radar altimeter (RA) to measure the height above ground level (AGL) and GPS WAAS information to derive the aircraft height above mean sea level (MSL). Because GPS and RA inputs are necessary for this method, failure of either one of these sensors would result in a failure of the integrity monitoring capability. Figure 5 illustrates the sensor measurements.

The difference between both sensor measurements is, ideally, equal to the height of the ground or terrain above MSL, that is the quantity that is stored in the terrain database. The synthesized height measurements are formed as:

$$h_{\text{syn}}(t_i) = h_{\text{GPS}}(t_i) - h_{\text{RA}}(t_i) - l_{ar} \tag{6}$$

where h_{GPS} is the height above MSL as derived from GPS/WAAS measurements, h_{RA} is the height AGL obtained from RA measurements, and l_{ar} is the distance offset between the GPS and the RA antennae, typically the distance between the roof and the belly of the aircraft. All measurements are referenced to time epoch t_i. To compare the database elevations and the elevations synthesized from the sensor measurements, a metric is chosen which is sensitive to bias

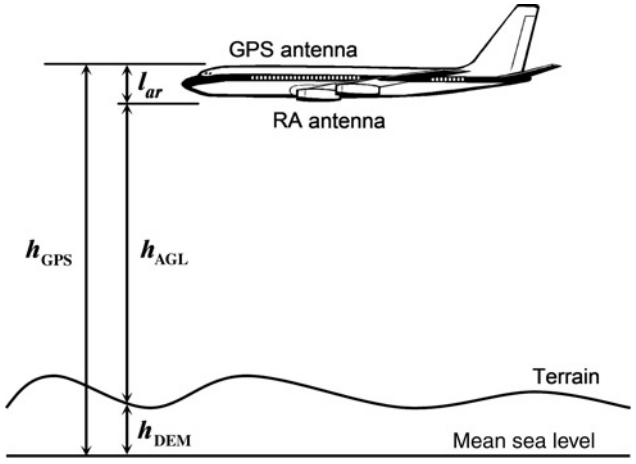

Fig. 5 Terrain profile measurements.

errors. This so-called consistency metric has been referred to as the absolute disparity (AD or p) in previous work, but is referred to as the sample disparity in this paper. The sample disparity is thus given by

$$x(t_i) = h_{\text{syn}}(t_i) - h_{\text{DEM}}(lat(t_i), lon(t_i)) \tag{7}$$

The expression $h_{\text{DEM}}(lat(t_i), lon(t_i))$ represents the DEM height lookup function for position coordinates (*latitude,longitude*) at time t_i. This height lookup function uses a bi-linear interpolation to estimate the DEM heights for horizontal coordinates that lie in between DEM-specified posts or values. Hence, the retrieved heights for closely spaced horizontal coordinates are highly correlated, just like the terrain would be. In a strictly statistical sense, [2] states that for an aircraft flying at a height of at least 290 m and a speed of no less than 60 m/s, the sample disparities, obtained by subtracting the digital terrain elevation database (DTED 1, $3'' \times 3''$ spatial resolution) terrain profile from the synthesized terrain profile, can be approximated as IID Gaussian random variables with mean zero (assuming no biases on the DTED) and a convolved standard deviation of 18.9 meters. The individual sensor standard deviations are shown in Table 2.

Because of the sensor measurement noise, the sample disparities are normally distributed as well. Thus, the expression for the integrity monitor T-value, T, follows the structure of Eq. (1)

$$T = \frac{1}{\sigma^2} \sum_{i=1}^{N} x^2(t_i) \tag{8}$$

To use this statistic for hypothesis testing and decision-making, an appropriate criterion or threshold must be computed such that, if T is below the threshold, the null hypothesis is accepted and if T is above the threshold, the null hypothesis is rejected and the alternate hypothesis is accepted (bias present). Within the context of this paper, P_{FFD} is chosen to be 10^{-4} and P_{MD} is specified as 10^{-7}. The number of degrees of freedom N is chosen to be equal to 50 and, thus, corresponds to 50 successive measurements. As mentioned earlier, P_{FFD} and N determine the threshold T_{th}, whereas T_{th} and P_{MD} can be used to find λ_{B}. To enable an efficient way to look-up different values for T_{th} and λ_{B}, figures such as Fig. 6 have been proposed. The top four curves in Fig. 6 allow the user to find T_{th} for four values of P_{FFD} given a predefined number of samples N. The lower four curves allow the user to find λ_{B} for four values of P_{MD} given the threshold found earlier. Using the given values for P_{FFD}, P_{MD}, and N, one can find the threshold value to be equal to $T_{\text{th}} = 96$ and the value of the noncentrality parameter to be equal to $\lambda_{\text{B}} = 164.17$. Using Eq. (5) with $\sigma = 18.9$ m, μ_B is found to be equal to 34.2 m, which means that it is still possible to accept $\mathbf{H}_0$ with a probability of P_{MD} if a bias of 34.2 meters or more is present.

The test statistic T_{KF} using the Kalman filter estimates of sample disparities is given as

$$T_{KF} = \frac{1}{P} \sum_{k=1}^{N} \hat{x}^2(t_k) \tag{9}$$

where the $\hat{x}$ values are the Kalman filter estimates of the sample disparities and P is their steady-state variance. The procedure for the vertical domain integrity monitor described above is summarized in Fig. 7.

B. Horizontal Domain Integrity Monitor

The concept of using downward-looking sensors for detection of horizontal failure modes was introduced in [3] and referred to as the multiple path downward looking integrity monitor (MPDLIM). In MPDLIM the T value is computed over multiple flight paths that are horizontally offset from the nominal flight trajectory (provided by the GPS positions). The horizontal offsets form a rectangular search grid around the nominal position at each time epoch. The T value at each position offset represents the measure of similarity between the terrain database profile below the offset flight path and the synthesized terrain profile. In essence, the vertical domain integrity monitor has been extended so that multiple terrain profiles from the terrain database would be compared to a single synthesized terrain profile. All the grid points whose associated T value does not exceed the integrity monitor threshold correspond to horizontal offsets (in the terrain database) that would remain undetected with a probability of the missed detection

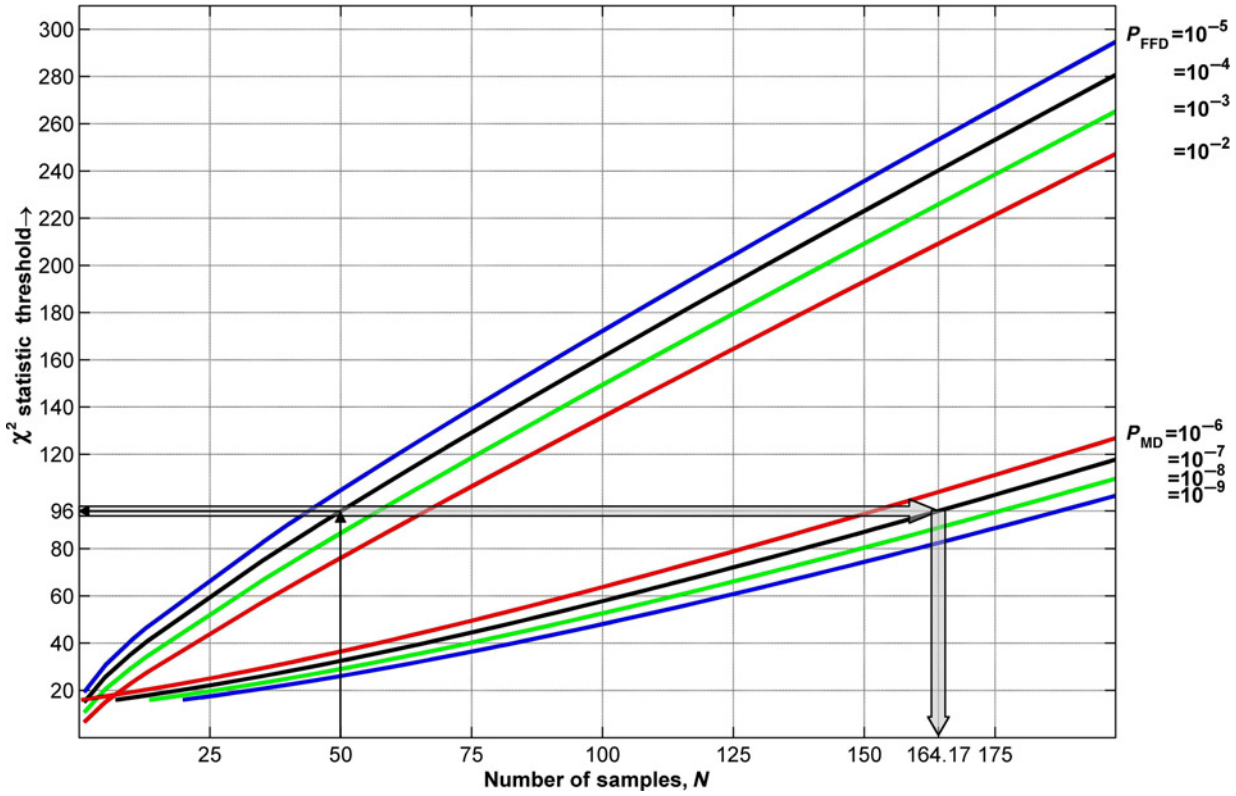

Fig. 6 χ^2 threshold and Noncentrality Parameter Lookup Plot.

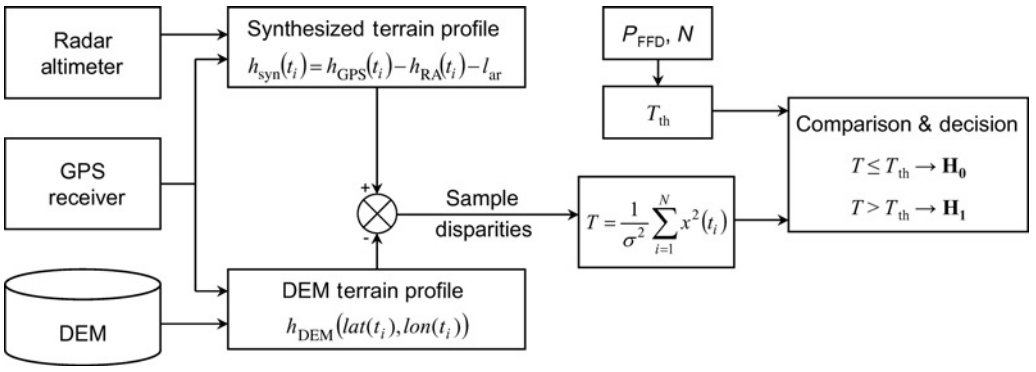

Fig. 7 Vertical domain integrity monitor block diagram.

probability or more. These grid points form the so-called region of missed detection (RMD). The expression for the test statistic T at all the horizontally offset grid points can be written in mathematical form as follows

$$T(m,n) = \frac{1}{\sigma^2}\sum_{i=1}^{N}(h_{\text{syn}}(t_i) - h_{\text{DEM}}(lat(t_i)+m, lon(t_i)+n))^2 \tag{10}$$

where m, n are the horizontal position offsets in latitude and longitude, having similar units. The variables m, n are varied in permutations ranging from, say, $-$L to $+$L, the maximum lateral offset, so as to cover the entire horizontal search grid. An illustration of MPDLIM is shown in Fig. 8.

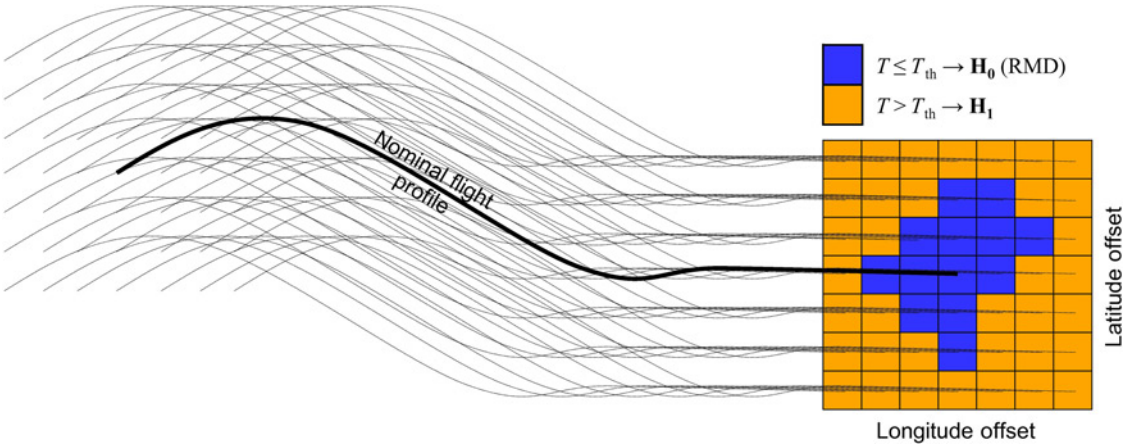

Fig. 8 Search grid and RMD for the horizontal domain integrity monitor.

The performance of the horizontal domain integrity monitor is a function of the terrain signature (roughness and nonperiodicity). The performance relies greatly on the deviation of the DEM terrain profile from the synthesized profile over the different points in the search grid. For terrain with a large spatial similarity such as flat or periodic terrain, the computed T values are similar over the entire search grid, resulting in decreased MPDLIM performance. However, while traversing such terrain, the CFIT risk is much smaller also. Rough, quickly varying and nonperiodic terrain offers improved performance of the horizontal integrity monitor and, in general, is associated with an increased risk of CFIT.

C. Spatial Domain Integrity Monitor

The horizontal domain integrity monitor is extended to include a vertical height bias to form a spatial integrity monitor, similar to the 'spatial envelope' shown in Fig. 2, by introducing an intentional vertical bias of increasing magnitude on the synthesized heights and applying the MPDLIM scheme to form RMDs corresponding to each vertical bias. The 3D grid of T values can be described mathematically as follows

$$T(m, n, b) = \frac{1}{\sigma^2} \sum_{i=1}^{N} (h_{\text{syn}}(t_i) - h_{\text{DEM}}(lat(t_i) + m, lon(t_i) + n) + b)^2 \tag{11}$$

where $b = -B$ to $+B$, the maximum vertical bias. Integrity monitor results in all three domains are shown in the next section.

V. Terrain Database Integrity Monitor Results

During a research flight test mission on January 14, 2005, we collected GPS and radar altimeter data, among other sensors. These data sets are used in this paper to demonstrate the integrity monitor and position estimation (described in later sections) performance. A total of eight precision approaches were flown into Braxton county regional airport (K48I) in West Virginia, aboard Ohio University's Douglas DC-3 aircraft, see Fig. 9. The approach profiles are shown in Fig. 10, overlaid on the terrain elevation profile.

The GPS sensor used was a NovAtel OEM4 receiver enabled for WAAS signals. The radar altimeter was a Honeywell HG8505 altimeter, operating at a measurement rate of 25 Hz. The DEM was the digital terrain elevation database (DTED) level 1, whose specifications are given in Table 3.

A. Vertical Domain Integrity Monitor

Corresponding to the theory detailed in the previous sections, the results of the integrity monitor using unfiltered and Kalman filtered sample disparities are presented here.

Fig. 9 Douglas DC-3 research aircraft used to fly the mission.

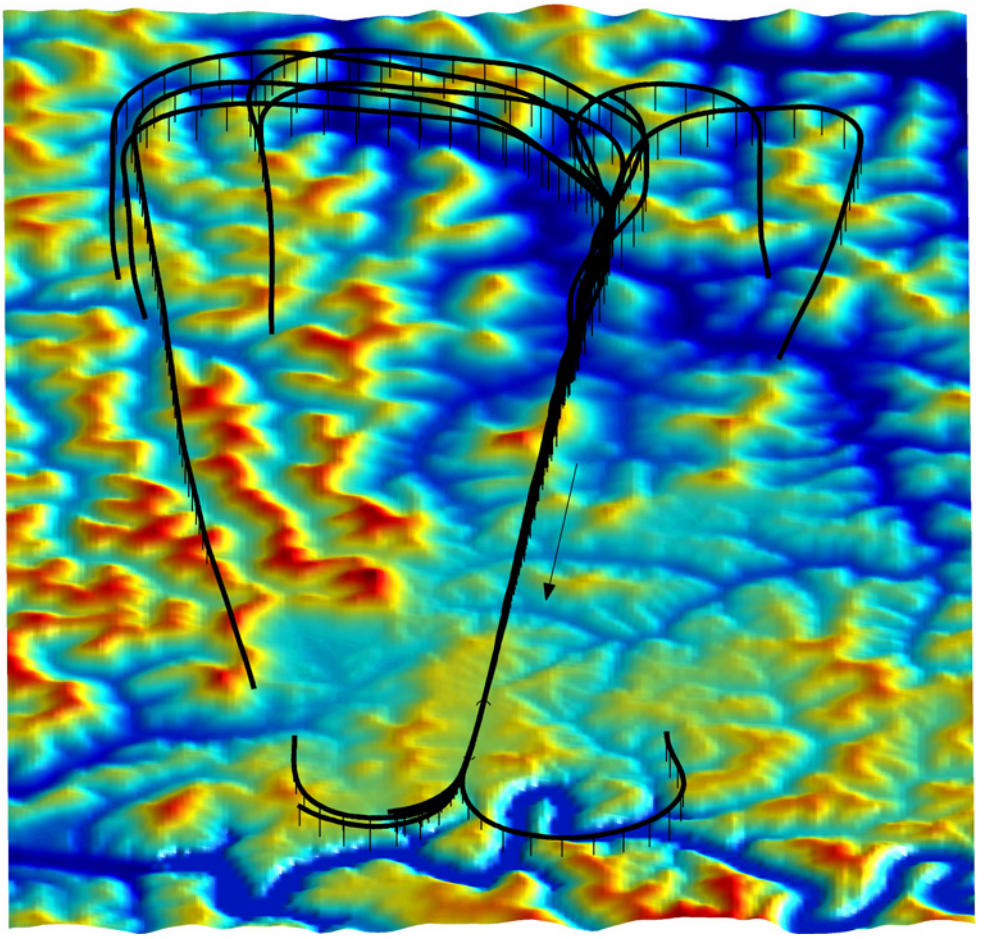

Fig. 10 Terrain elevations and flight profile over eight approaches to runway 19 at K48I.

Table 3 DTED level 1 specification [4]

Post spacing	Absolute vertical accuracy	Absolute horizontal accuracy	Vertical datum	Horizontal datum
3 arc-seconds	<30 m, 90% L.E.P	<50 m, 90% C.E.P	MSL	WGS84

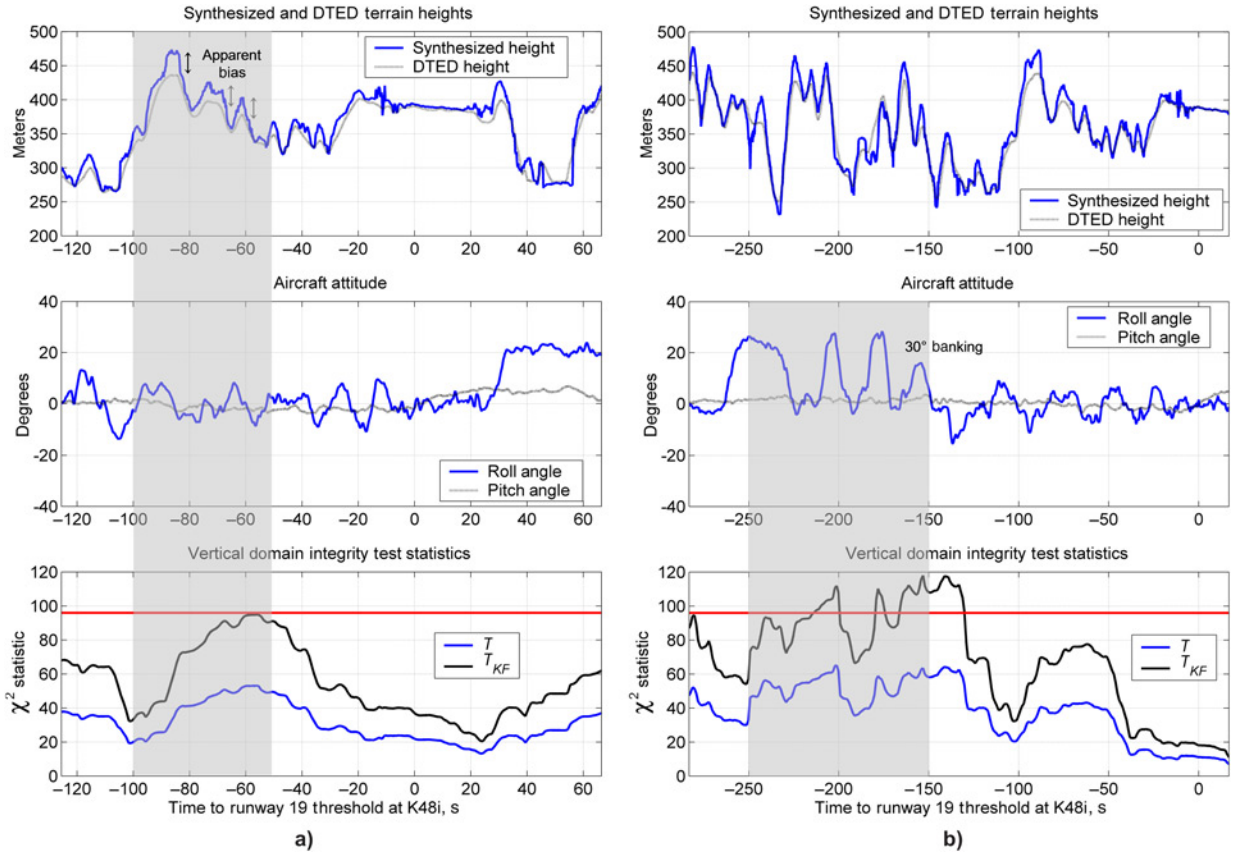

Fig. 11 Sample vertical domain integrity monitor performance.

Figure 11 (set of three sub-plots on the left (11a) and right (11b) are two different approach cases) are examples of comprehensive plots of the synthesized and DTED elevations, the vehicle attitude and T values for the unfiltered and Kalman filtered cases from two of the eight test approaches. These two flight test segments were selected to demonstrate two unique phenomenons that affect the T values. The first, of course, is the presence of a bias that causes an increase in the value of the T statistic. As evidenced from Fig. 11a, in the gray shaded portion, the synthesized and DTED terrain profiles consistently do not agree contributing to an apparent bias that causes the T and T_{KF} values to increase, though still within the threshold limit. The second phenomenon is a radar altimeter 'slant height' measurement, owing to adverse aircraft banking. When the aircraft banks steeply, instead of measuring the 'plumb-bob' height, the radar altimeter measures a slant height that is different from the actual height AGL. The slant height can be greater or lesser than the actual height AGL depending on the terrain underneath the aircraft. For example, over relatively flat terrain (nearly constant terrain elevations), the slant height will be greater than the plumb-bob height, whereas, if the aircraft is banking away from a mountain and the radar altimeter illuminates the side of the mountain, the slant height will be lesser than the plumb-bob height. The slant height measurements contribute to discrepancies between the synthesized and DTED heights that look like biases over the time interval it takes the aircraft to execute and complete the turn and increase the value of the test statistic during that time. This effect is clearly observed in Fig. 11b. The vertical domain integrity monitor performance over all eight approach flight segments is shown in Fig. 12. Note the consistency of the test statistics from time index -100 to $+50$ when aircraft is on final approach.

B. Horizontal Domain Integrity Monitor

The multiple path search (MPDLIM) described in Sec. IV.B for quantifying the integrity monitor's sensitivity to horizontal errors in the DEM was applied to the flight test data, and presented here. For the flight profile and vertical

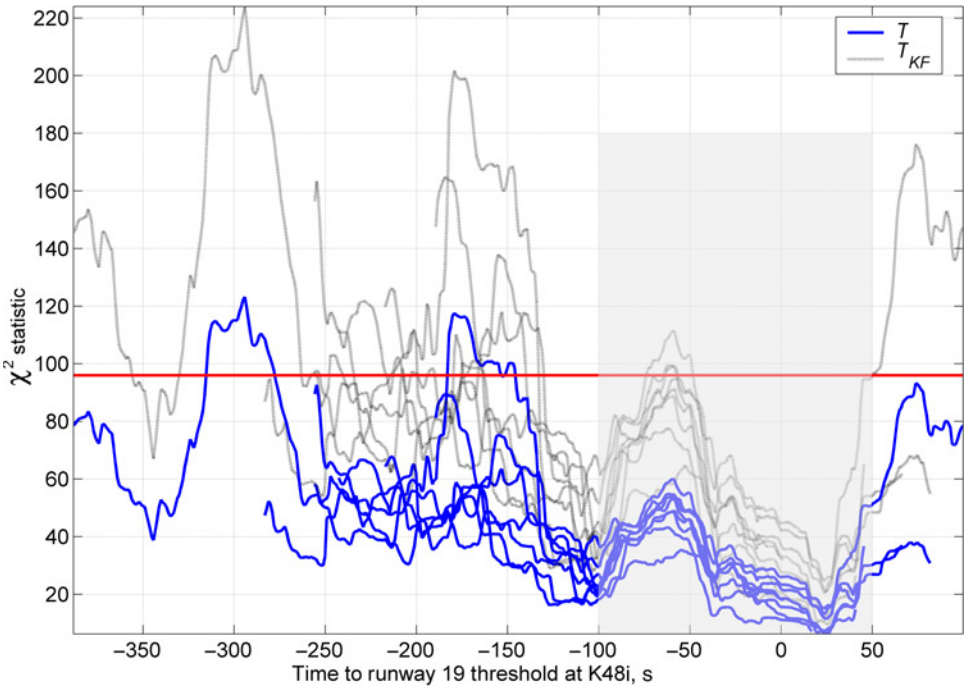

Fig. 12 Vertical domain integrity monitor performance.

domain results corresponding to Fig. 11a, the regions of missed detection (RMD, or position uncertainty) at four selected times are shown in Figs. 13a and 13b.

In Fig. 13a, the RMD was computed using unfiltered sample disparities and the T statistic. Fig. 13b used Kalman filtered disparities and the T_{KF} statistic. It is clearly seen that even in the horizontal domain, the Kalman filter reduces the position uncertainty or RMD and improves the horizontal bias performance of the integrity monitor. The times indicated above the plots are the times to runway 19 threshold crossing, with negative values indicating that the aircraft is approaching the runway and positive values indicating that the aircraft has crossed and flying past the runway threshold. Representation of RMD as in Fig. 13 is ideal for comparisons at a specific time epoch. However, to gauge the performance over the entire flight path (and representation on paper), the total area of RMD within approximately a 1 km $\times$ 1 km grid at 1 s intervals over all eight approach segments is shown in Fig. 14.

Note the increase in RMD as the aircraft approaches the runway. This occurrence can be explained by considering the terrain signature or gradient. The terrain around the runway is the rolling hills of the Appalachian ranges which present a high terrain gradient. However, as one approaches the runway, the terrain flattens out and has a lower gradient, which explains the increased position uncertainty in the horizontal direction and the higher RMD. To quantify the terrain gradient, it can be expressed by the following metric

$$\mathrm{TGM} = \sqrt{\frac{1}{N}\sum_{i=2}^{N}\left(h_{\mathrm{syn}}(i) - h_{\mathrm{syn}}(i-1)\right)^2} \tag{12}$$

Figure 15a shows a plot of the variation of the terrain gradient metric (TGM) over the flight path. A different color corresponds to each of the eight approach flight segments. Fig. 15b substantiates the above explanation regarding the inverse relation between the RMD and TGM.

C. Spatial Domain Integrity Monitor

In this section, we extend the horizontal domain integrity monitor by also including vertical height offsets and form the "spatial envelope" of missed detection, in other words, the 3D region of position uncertainty. Again, for the

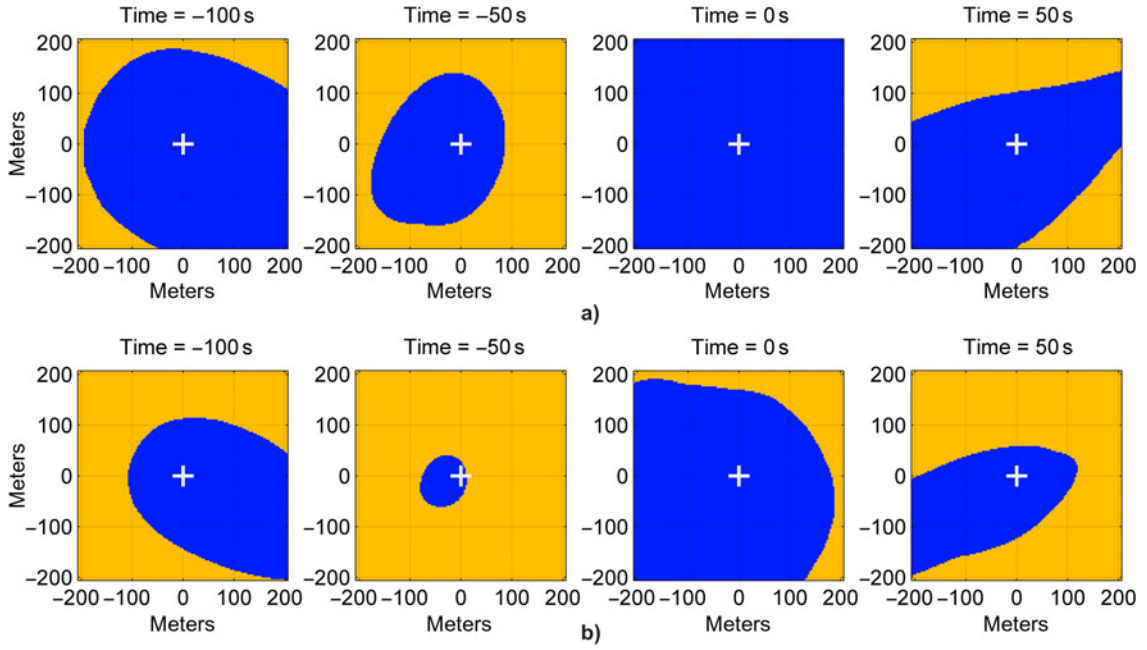

Fig. 13 a) Regions of missed detection (RMD) using unfiltered disparities and T statistic. b) Regions of missed detection (RMD) using Kalman filtered disparities and T_{KF} statistic.

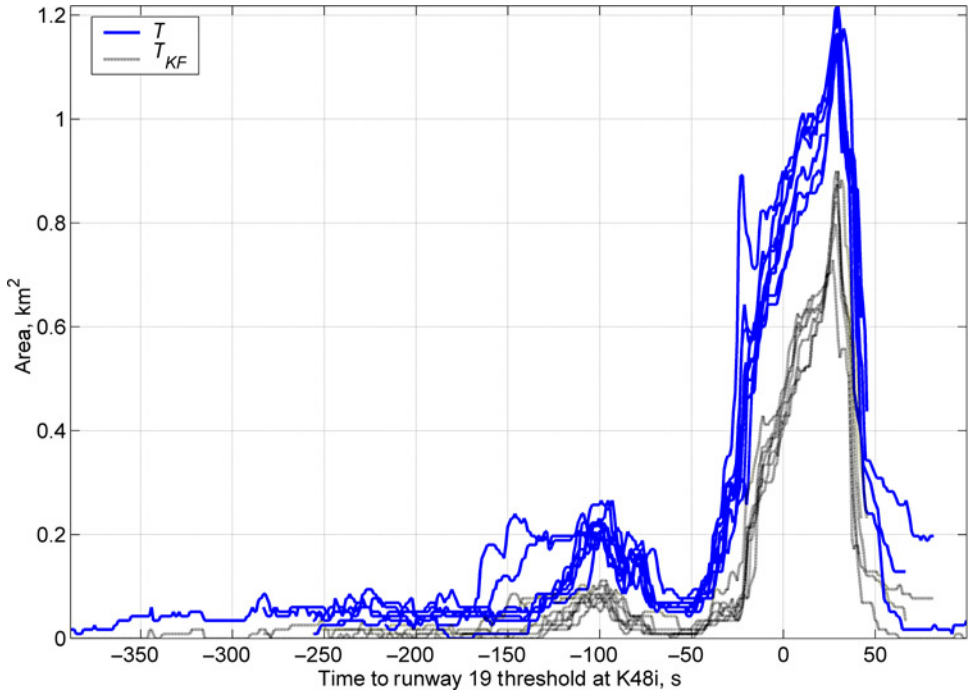

Fig. 14 Horizontal domain integrity monitor performance.

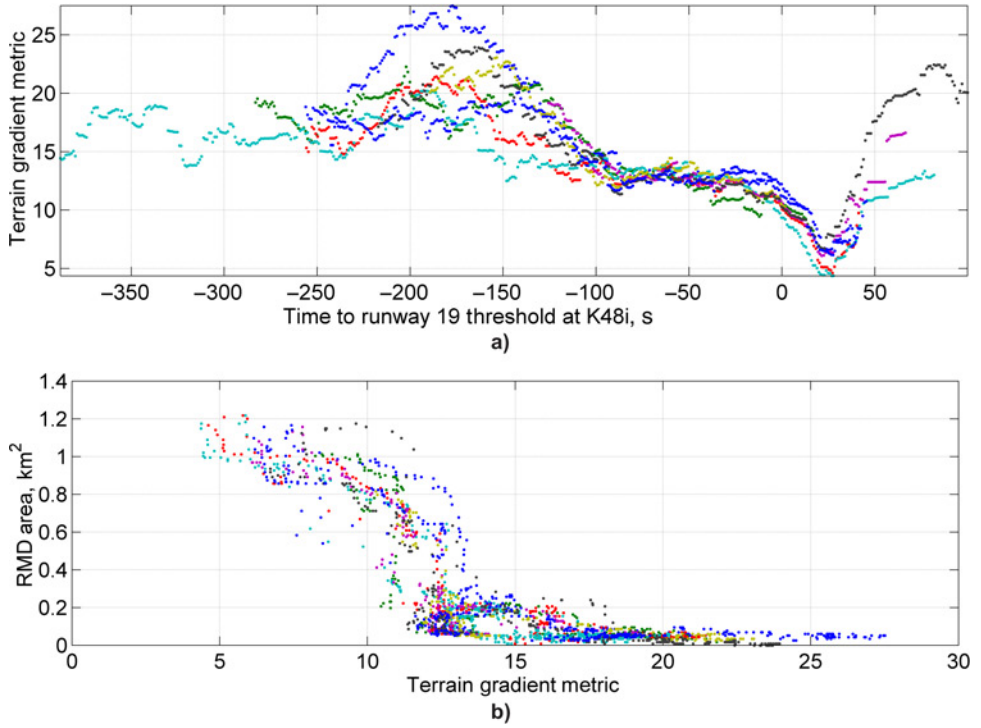

Fig. 15 a) Terrain gradient metric over eight flight approaches to runway 19. b) RMD as a function of the terrain gradient metric.

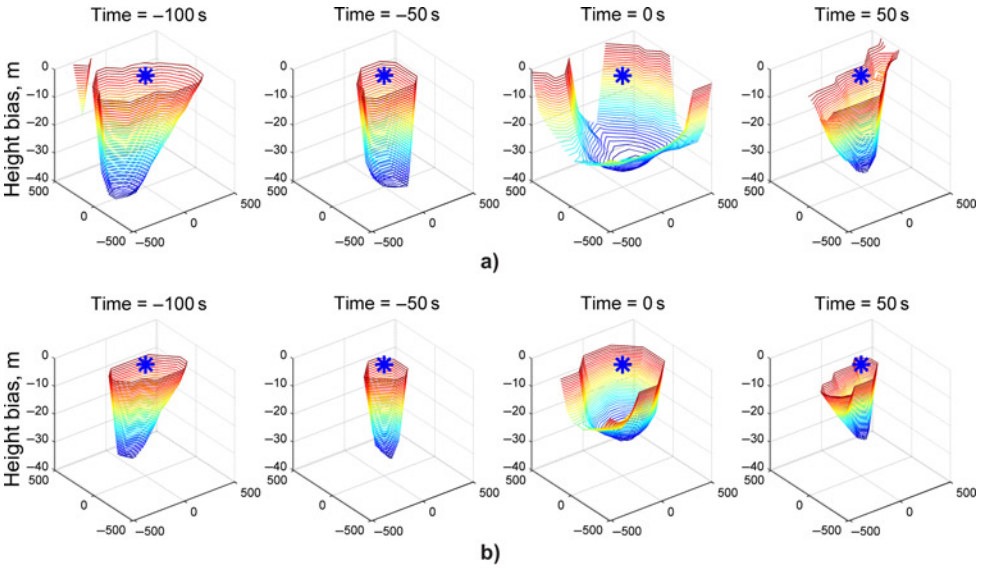

Fig. 16 a) Spatial envelope using unfiltered disparities and T statistic. b) Spatial envelope using Kalman filtered disparities and T_{KF} statistic.

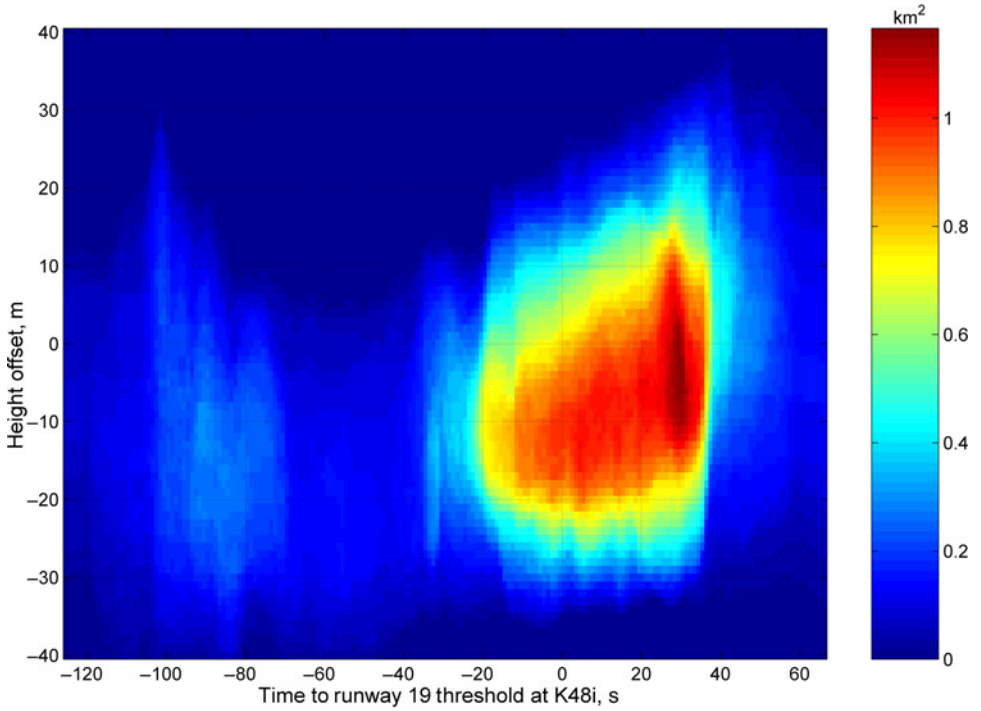

Fig. 17 RMD as a function of height offset over an approach flight segment.

same flight profile and times corresponding to Fig. 11a, and Fig. 13, the spatial envelope at the four selected times is shown in Figs. 16a and 16b.

The units on all axes are meters although the vertical axis is scaled differently for visualization purposes. A reduction in the extent of the spatial envelope at all four locations is observed by the use of a Kalman filter. Note how the space envelopes taper off with increasing magnitudes of vertical biases as more points exceed the T statistic decision threshold. Also, the contours do not extend beyond 35 m for the unfiltered case and beyond 25 m for the Kalman filtered case, which are their respective minimum detectable biases.

Because of challenges of data representation, we do not show the spatial envelope contours over the entire flight path; instead, the horizontal RMD is represented as a color-coded image and plotted versus time and height offset, in Fig. 17.

VI. Terrain Database Referenced Navigation

In this section, we present a terrain database-referenced navigation scheme that can be performed simultaneously with the spatial integrity monitor function. The results of the spatial integrity monitor show that there exists a unique minimum T value within the spatial envelope. The minimum T value implies that the sensor measurements and the terrain database are in best agreement at that particular location (position coordinates), with respect to the database. Because GPS is an enabling sensor for the operation of the integrity monitor, and GPS provides good position estimates of the aircraft, an additional navigation or position estimation scheme may seem redundant. To explain the necessity for such an addition, we refer back to the motivation for this research. Remember that the terrain database is used for generating the display imagery for SVS and an integrity monitor may be required for the detection of biases on the terrain database. In the event a bias is detected, the terrain imagery in the SVS can either be removed from the display or corrected in some way to ensure continuity of the SVS display. Although GPS provides absolute position information, in the context of an SVS display, we are interested in the aircraft position with respect to a *possibly biased* terrain database, so that the visual information is not misleading to the pilot.

Figure 18 illustrates the scheme for a DEM-referenced spatial position estimator that estimates the horizontal translation (north and east or latitude and longitude) as well as a vertical bias offset. The algorithm identifies the

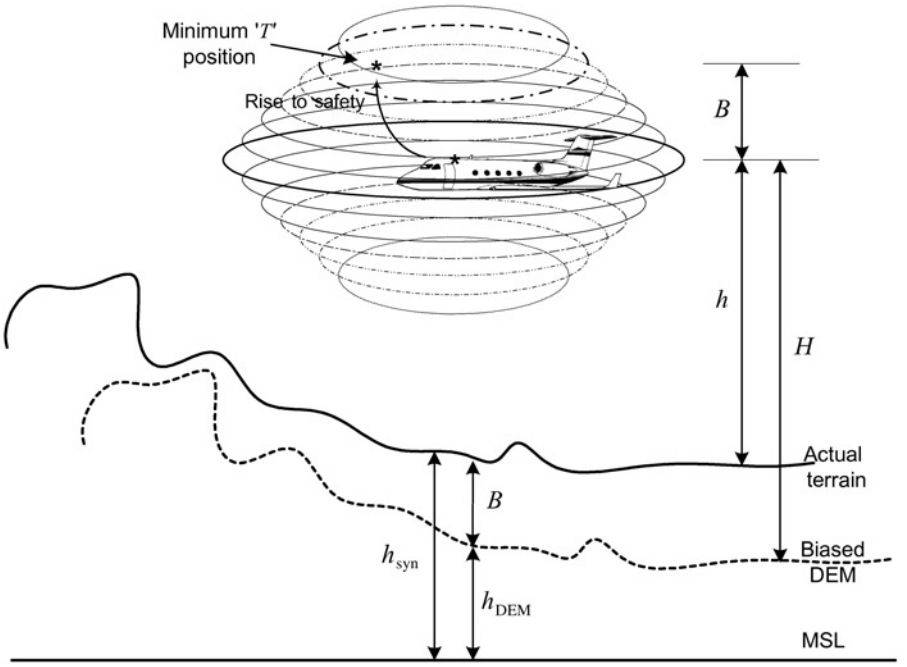

Fig. 18 Illustration of terrain database referenced spatial position estimation.

position that corresponds to the minimum T value within the spatial envelope and computes the north, east, and vertical offsets from the true GPS position.

An explanation of the proposed method and a few definitions are in order. Consider an aircraft navigating with respect to a biased DEM that has a profile below the actual terrain. Consider, furthermore, that this bias is equal to 'B'. If the aircraft intends to maintain a constant altitude 'H' above the terrain and relies on the DEM for situational awareness, the aircraft will actually have a terrain clearance of $h = \mathrm{H} - B$. This situation can lead to an increased risk of CFIT in challenging terrain environments as illustrated in Fig. 18. The spatial position estimation scheme identifies the most probable aircraft position (with reference to the DEM), by introducing a set of intentional positive and negative vertical biases on the synthesized elevations and computing the T values over a horizontal search grid corresponding to each vertical bias. In this way, a spatial envelope of T values is computed in a fashion similar to the space envelope discussed in Sec. V.C. Next, the minimum T value is identified within this 3D grid of points and the position corresponding to the minimum T value is identified as the most probable aircraft position. The difference between the *spatial integrity monitor* and the *spatial position estimation* schemes is that the former compares all the T values to a threshold while the latter identifies the minimum.

In the proposed method, a *positive bias* is defined as a potentially dangerous bias that could result in an increased risk of CFIT. A DEM is said to have a positive bias when the DEM profile is lower than the actual terrain profile. An aircraft relying on the DEM assumes it is further away from the terrain than is the case. In the presence of such a positive bias, the aircraft must rise higher to increase its level-of-safety.

A *negative bias* is defined as a bias that could result in a so-called loss of terrain. A negative bias exists when the DEM profile is higher than the actual terrain profile. Although a negative bias does not increase the probability of CFIT, it could be potentially dangerous for operations that require the aircraft to be in proximity to the ground, such as precision approach and landing.

VII. Terrain Database Referenced Navigation Results

The absolute vertical accuracy of the DTED level 1 terrain database is specified as $<$30 m 90% and its horizontal accuracy as $<$50 m 90% (Table 3). Using these numbers as reference, intentional biases of 30 m in the vertical and

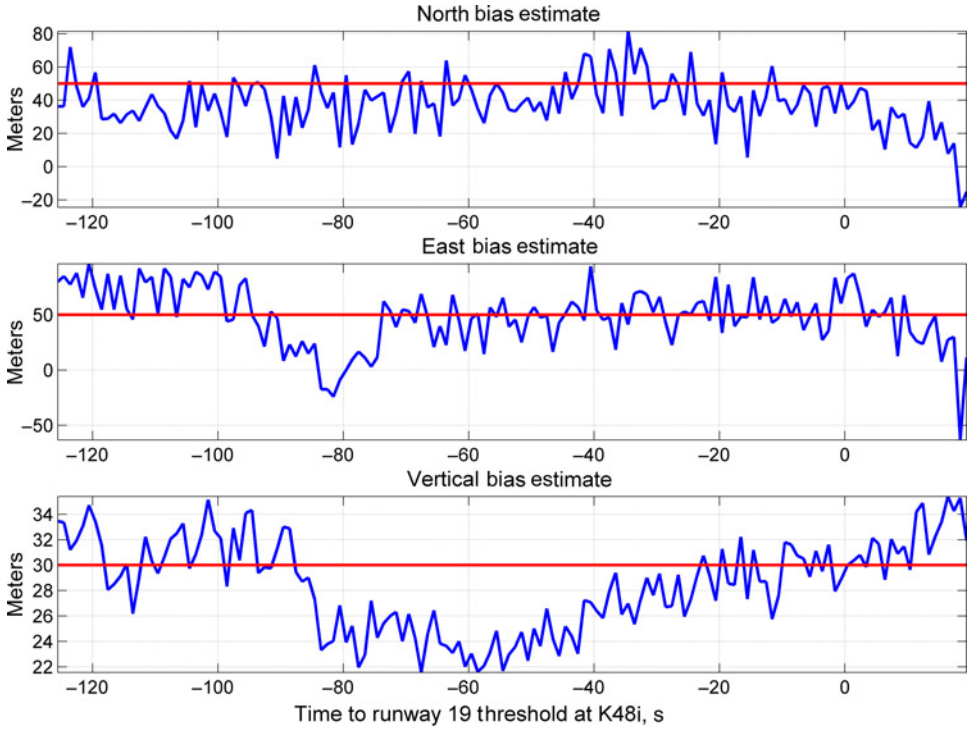

Fig. 19 Estimates of DEM Biases over an approach flight.

50 m in each of the horizontal axes were introduced in the DEM. The spatial position estimation method using the T value (Eq. 8) was used and the position solution results are presented in this section.

Figure 19 shows the position offsets in north, east, and vertical axes of the navigation frame that were determined to be the most likely position offsets and corresponded to a minimum T value. The search was conducted with a vertical resolution of 1m and a horizontal resolution of 30 m (1 arc-sec.) which is smaller than the DEM resolution of approximately 90 m (3 arc-secs.). To minimize errors owing to quantization, the search was initialized with a different random offset each time. As we can see from Fig. 19, the minimum T metric method was able to estimate the biases to within 10–15 m, which is quite good given the DEM resolution. Further results from all eight approach flights and their mean position bias estimates are provided in the figures below and summarized in Table 4. The flight data used for bias estimation were restricted to benign dynamics, i.e. roll and pitch angles less than 20° to minimize the effects of radar altimeter slant height measurements. The effect of height discrepancies between the synthesized and DEM heights, along with some slant height measurement effects (roll and pitch $\leqslant$20°) can still be observed owing to the large variance of the scatter plots of Fig. 20. The red plus sign '+' corresponds to the intentionally

Table 4 Mean and standard deviation of bias estimation error

	Mean, m			Standard deviation, m		
	North	East	Vertical	North	East	Vertical
Flt. 1	1.67	−1.01	0.99	27.07	32.91	3.28
Flt. 2	−0.19	0.42	0.05	29.66	25.35	3.60
Flt. 3	−11.53	−14.00	−1.40	20.22	22.19	3.19
Flt. 4	−3.52	−9.80	0.73	29.07	36.99	5.39
Flt. 5	−12.35	−1.38	−1.52	15.99	26.93	3.59
Flt. 6	−9.27	1.42	−0.33	16.62	15.70	2.74
Flt. 7	−18.67	−4.23	−2.31	17.83	17.72	2.33
Flt. 8	−6.05	0.60	1.08	25.41	27.64	5.00

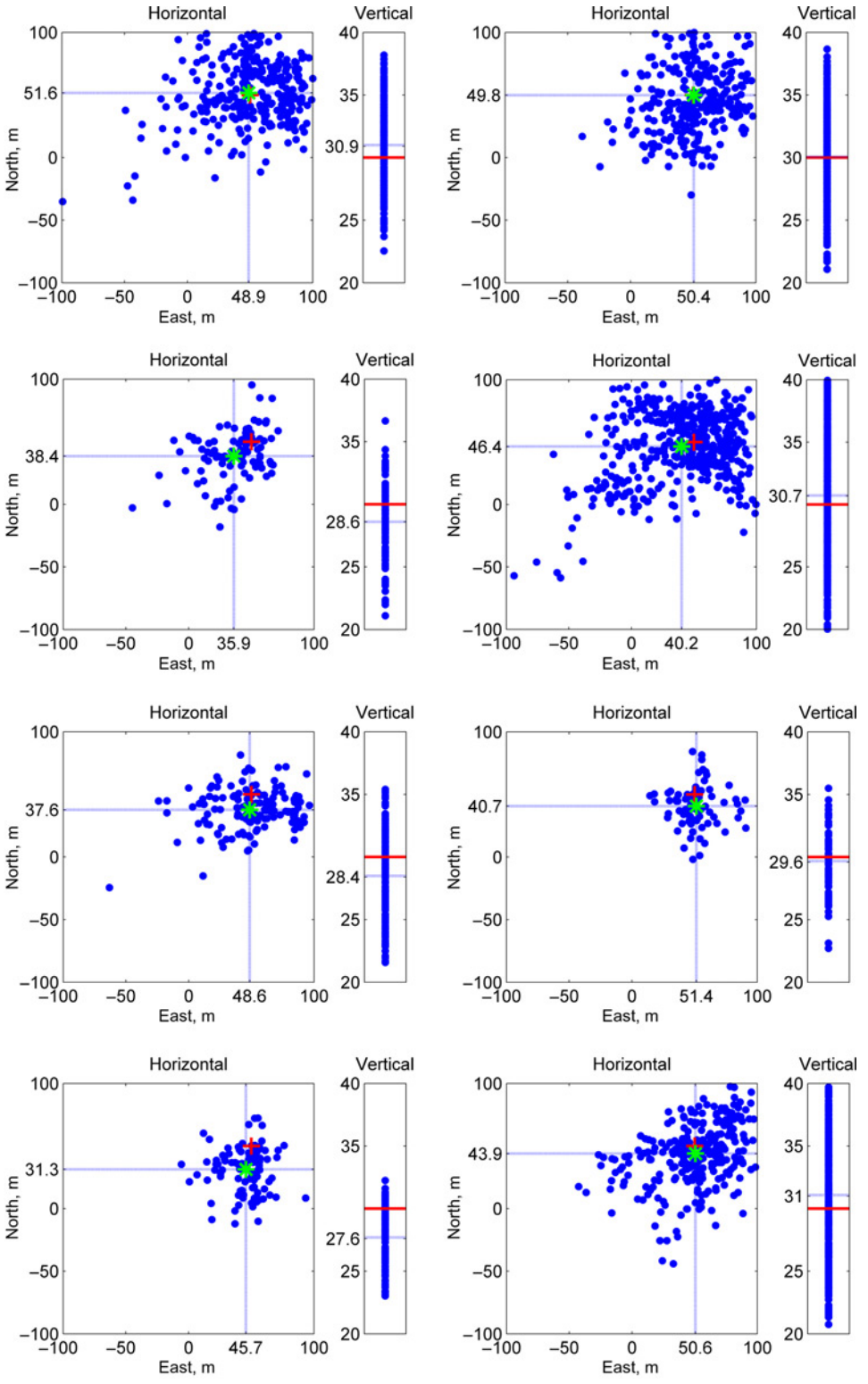

Fig. 20 Scatter plots of horizontal and vertical bias estimates.

introduced horizontal bias coordinates (50 m, 50 m), and the green star '*' corresponds to the mean coordinates of the scatter points.

VIII. Summary and Conclusions

A terrain database integrity monitor may be a necessary component of synthetic and enhanced vision systems to support intended functions that require FAA system certification to levels that are more stringent than advisory. The digital terrain database is an important component of the system that provides terrain information for the SVS display. If the integrity of the terrain database is not guaranteed by the terrain database providers at the time of generation, it is necessary to include an integrity monitor during operation by the user. The integrity monitor uses sensors that already exist on most aircraft, namely, GPS receiver and radar altimeter, hence, the inclusion of the integrity function will require minimal additional hardware. In this paper, we reviewed the development of a 3D spatial integrity monitor and presented results using flight test data collected aboard Ohio University's DC-3 aircraft in the vicinity of Braxton County Airport, WV.

Statistical characterization of the vertical domain integrity monitor with regard to its minimum detectable bias is straightforward, so the same concepts have been extended to the horizontal and the spatial domains. The extension lies in the fact that, although the measurements are in the Height domain, they have been used to detect horizontal biases in the DEM. However, an additional parameter that influences the horizontal bias detection capability is the terrain signature. We presented results that illustrate the relation between the terrain signature or gradient and the integrity monitor's horizontal performance. A Kalman filter was designed and applied to the sample disparities in an attempt to reduce the noise level and estimate a potential bias. It is observed that under acceptable tradeoffs, the performance of the integrity monitor is greatly improved using the Kalman filter method.

The spatial integrity monitor concept has been extended to terrain database referenced navigation also. The principle behind this is that if a terrain database bias does exist, in addition to raising an integrity alert, the aircraft location with respect to the DEM is estimated and the SVS display can be corrected to depict the correct outside-world perspective. The position estimation method uses the same χ^2 test statistic used for integrity monitoring and hence both functions can be performed together. We observed that the mean vertical position estimates were within 5 m of the truth, given the quality of sensors and DEM. The mean horizontal position estimates were within 10–15 m of the truth, and more precise position estimates require closer spacing of the search grid points which in turn require a higher resolution DEM. For further improvement in the performance of both functions, algorithms to compensate or properly account for the radar altimeter slant height measurements must be developed.

Acknowledgments

The work presented in this paper was partly supported and funded by NASA through cooperative agreement NCC-1-351. We thank the Ohio University DC-3 flight crew, pilots Richard McFarland and Bryan Branham, and technical support staff Jay Clark and Paul Nilles for their help with the flight tests.

References

[1] Williams, D. M., Waller, M. C., Koelling, J. H., Burdette, D. W., Capron, W. R., Barry, J. S., Gifford, R. B., and Doyle, T.M., "Concept of Operations for Commercial and Business Aircraft Synthetic Vision Systems – Version 1.0," NASA/TM-2001-211058, December 2001.

[2] Gray, R. A., "Inflight Detection of Errors for Enhanced Aircraft Flight Safety and Vertical Accuracy Improvement Using Digital Terrain Elevation Data With an Inertial Navigation System, Global Positioning System and Radar Altimeter," Ph.D. Dissertation, Ohio University, Athens, OH, June 1999.

[3] Campbell, J. L., "Characteristics of a Real-Time Digital Terrain Database Integrity Monitor for a Synthetic Vision System," M.S.E.E. Thesis, Ohio University, Athens, OH, November 2001.

[4] "Performance Specification: Digital Terrain Elevation Data (DTED)," MIL-PRF-89020B, May 23, 2000.

[5] Uijt de Haag, M., Young, S., and Gray, R., "DTED Integrity Monitoring Using Differential GPS and Radar Altimeter," *Proceedings of the IAIN World Congress in Association with the U.S. ION Annual Meeting*, ION, San Diego, CA, June 2000, pp. 820–830.

[6] Uijt de Haag, M., Sayre, J., Campbell, J., Young, S., and Gray, R., "Flight Test Results of a Synthetic Vision Elevation Database Integrity Monitor," *Proceedings of SPIE*, Vol. 4363, Enhanced and Synthetic Vision, 2001, pp. 124–133.

[7] Campbell, J., Uijt de Haag, M., Vadlamani, A., and Young, S., "The Application of LiDAR to Synthetic Vision System Integrity," *Proceedings of the 22nd Digital Avionics Systems Conference (DASC)*, IEEE/AIAA, Indianapolis, IN, 2003, pp. 9C2.1-7.

[8] Young, S. D., and Uijt de Haag, M., "Detection of Digital Elevation Model Errors Using X-band Weather Radar," *Journal of Aerospace Computing, Information, and Communication*, published online, Vol. 2, No. 8, 2005, pp. 309–326. doi: 10.2514/1.13567

[9] Golden, J. P., "Terrain Contour Matching (TERCOM): A Cruise Missile Guidance Aid," *Proceedings of SPIE, Vol. 238*, Image Processing for Missile Guidance, 1980, pp. 10–18.

[10] Baird, C. A., and Abramson, M. R., "A Comparison of Several Digital Map-Aided Navigation Techniques," *Proceedings of the IEEE Position, Location and Navigation Symposium*, Inst. of Electrical and Electronics Engineers, New York, NY, 1984, pp. 286–293.

[11] Hostetler, L. D., and Beckman, R. C., "The Sandia Inertial Terrain-Aided Navigation System," Sandia Laboratories, SAND77-0521, Springfield, VA, September 1977.

[12] Hostetler, L. D., and Andreas, R. D., "Nonlinear Kalman Filtering Techniques for Terrain-Aided Navigation," *IEEE Transactions on Automatic Control*, AC-28, March 1983, pp. 315–323. doi: 10.1109/TAC.1983.1103232

[13] Runnalls, A. R., "A Bayesian Approach To Terrain Contour Navigation," AGARD Unclassified paper No. 43, Guidance and Control Panel, 40th Symposium, May 1985, pp. 43-1–43-25.

[14] Vadlamani, A., and Uijt de Haag, M., "Improving the Detection Capability of Spatial Failure Modes Using Downward-Looking Sensors in Terrain Database Integrity Monitors," *Proceedings of the 22nd Digital Avionics Systems Conference (DASC)*, IEEE/AIAA, Indianapolis, IN, 2003, pp. 9.C.5.1-12.

[15] Vadlamani, A. K., and Uijt de Haag, M., "Improved Downward Looking Terrain Database Integrity Monitor and Terrain Navigation," *Proceedings of the IEEE Aerospace Conference*, Inst. of Electrical and Electronics Engineers, New York, NY, 2004, Paper 1545, pp. 1–14.

[16] Vadlamani, A. K., "Performance Improvement Methods for Terrain Database Integrity Monitors and Terrain Referenced Navigation," M.S.E.E. Thesis, Ohio University, Athens, OH, March 2004.

[17] Vadlamani, A. K., and Uijt de Haag, M., "A 3-D Spatial Integrity Monitor for Terrain Databases," *Proceedings of the 23rd Digital Avionics Systems Conference (DASC)*, IEEE/AIAA, Salt Lake City, UT, 2004, pp. 4.C.2.1-13.

[18] Johnson, R.A., *Miller and Freund's Probability and Statistics for Engineers*, 5th ed., Prentice-Hall, Upper Saddle River, NJ, 1995, pp. 271–273.

[19] Kay, S. M., *Fundamentals of Statistical Signal Processing, Volume II: Detection Theory*, Prentice-Hall, Upper Saddle River, NJ, 1998, pp. 20–28.

[20] Brown, R. G., and Hwang, P. Y. C., *The Discrete Kalman Filter, State-Space Modeling, and Simulation, Introduction to Random Signals and Applied Kalman Filtering*, 3rd ed., Wiley, New York, NY, 1997, pp. 190–241.

James Hargrave
Associate Editor